Supplimentary Online Material: Lattice Thermal Conductivity of Lower Mantle Minerals and Heat Flux from Earth's Core

M. A. G. M. Manthilake, N. de Koker, D. J. Frost, C. A. McCammon

S1 Sample Preparation

S1.1 Ferropericlase

Ferropericlase (FPe) samples were prepared using as starting materials magnesium and ferric oxides mixed in the desired mole ratios. These oxide mixtures were cold pressed into thin pellets, and kept at 1573 K in a gas mixing furnace for 24 hours. The oxygen fugacity of the sample was kept at two log units below the FMQ-buffer by adjusting the the CO_2/CO gas mixure in the furnace. Samples were then quenched in water and analyzed by X-ray powder diffraction to indentify the phases present. This procedure was repeated until pure ferropericlase was obtained (usually 2 - 3 times). The synthesised ferropericlase powder was hot pressed in an Fe-foil capsule at 5 GPa and 1073 K in a multi-anvil apparatus for about 30 minutes to obtain a well-synthesized cylindrical sample for thermal diffusivity measurements.

Prior to thermal diffusivity measurements, analysis by Mössbauer spectroscopy indicated $Fe^{+3}/\sum Fe$ of 2.6±1.5 for X_{Fe}=0.05 and 3.6±1.5 for X_{Fe}=0.2. Characterization by X-ray diffraction following the measurements indicated all ferropericlase samples to be single phase, and chemical composition was confirmed by electron probe microanalysis. Mössbauer spectroscopy indicate Fe^{+3} concentrations smaller than the uncertainty of measurement.

S1.2 Silicate Perovskite

Three perovskite compositions, $MgSiO_3$, $MgSiO_3$ + 3% $FeSiO_3$, and $MgSiO_3$ + 2% $AlAlO_3$ were synthesized for thermal diffusivity measurements. Synthesis of perovskite samples involved several steps. First, a glass was prepared by mixing oxides in the desired mole ratios and heating to 1923 K in an atmospheric furnace. $MgSiO_3$

+ 3% $FeSiO_3$ glass powder was subsequently reduced in a gas mixing furnace with a H_2/CO_2 gas mixture at 1473 K. These glass samples were hot pressed at 5 GPa and 1473 K in a multi-anvil apparatus to synthesize polycrystalline enstatite, which was then used to synthesize perovskite at 26 GPa and 1973 K.

Synthesised perovskite samples were characterized by both Raman spectroscopy and density measurements prior to thermal diffusivity measurements. After measurements were completed samples were again characterized by X-ray powder diffractometry and electron probe microanalysis to confirm the presence of a single phase. Mössbauer spectroscopy of the Fe-bearing perovskite indicated $Fe^{+3}/\sum Fe$ of 19.0±4.0.

S2 Experimental Method

Measurements of thermal diffusivity were performed using the Ångström method (e.g. Fujisawa et al., 1968), in which a sinusoidally varying temperature with angular frequency $\omega = 2\pi f$ is applied to the circumference of a cylindrical sample, and the phase lag (Φ) and amplitude ratio (Θ) in the temperature signal measured at radii r_1 and r_2 in the sample. Thermal diffusivity D is determined by solving

$$\Phi = \Phi_{r_1} - \Phi_{r_2} = \tan^{-1}\left[\mathrm{bei}(u)/\mathrm{ber}(u)\right], \tag{S1}$$

$$\Theta = \frac{\Theta_{r_1}}{\Theta_{r_2}} = \frac{1}{\sqrt{\mathrm{bei}^2(u) + \mathrm{ber}^2(u)}}, \tag{S2}$$

$$u = (r_2 - r_1)\sqrt{\frac{\omega}{D}}. \tag{S3}$$

for u, with $\mathrm{ber}(u)$ and $\mathrm{bei}(u)$ the real and imaginary Kelvin functions (e.g. Zhang and Jin, 1996). Thermal conductivity is then obtained as $\mathcal{K} = \rho C_P D$. To compute ρ and C_P at P and T, and to adjust $r_2 - r_1$ for the effect of compression, a thermodynamic model is used (see below).

Sample dimensions used for the measurements were 3.5 mm in diameter and 3.5 mm in length for ferropericlase, and 2.5 mm in diameter and 2.5 mm in length for perovskite. Pre-synthesized cylindrical samples were cut into two halves along the axial direction and a vertical groove made to accommodate an inner thermocouple; the outer thermocouple was placed along the surface of the sample. Thermocouples were fabricated from 0.05 mm diameter $W_{97}Re_3$-$W_{75}Re_{25}$ wires.

Measurements were performed using the 5000 tonne press at the Bayerisches Geoinstitut (Frost et al., 2004). For measurements of ferropericlase at 8 and 14 GPa, we used a 25/15 multi-anvil configuration (Figure S1). Measurements of perovskite

samples were performed using a modified 18/8 configuration at 26 GPa, which allowed the measurement to be made within the stability field of silicate perovskite. A stepped geometry was used for the furnace to reduce the temperature gradient in the axial direction and minimize the axial heat flow. The furnace was supplied with a 1 KHz alternating current, with a superimposed low-frequency modulation of the heater current to generate the temperature oscillation needed for thermal diffusivity measurements. Modulation frequencies of 0.1, 0.4, 0.7, 1.0 and 1.3 Hz were used for this.

The experimental procedures for thermal diffusivity measurements were as follows. Samples were first compressed at room temperature to the desired pressure. Once the assemblage is stable at this pressure, the thermal conductivity is measured as a function of temperature. In the case of ferropericlase, diffusivity measurements were made during heating and cooling in 100 K steps up to 1273 K; for perovskite samples were first heated to 1273 K, with thermal diffusivity measured made during cooling. At each temperature, samples were allowed to reach steady state before measurements were taken (Figure S2). Amplitude and the phase at each modulation frequency were obtained by fitting 10 sinusoidal cycles to the fitting equation,

$$T_r = T_r^0 + T_r^1 t + \Theta_r \sin(\omega t + \Phi_r). \tag{S4}$$

where T is temperature, t time, and ω, Θ_r and Φ_r are angular frequency, amplitude and phase of the temperature oscillation, respectively. Amplitude ratio Θ and phase shift Φ were then calculated by dividing inner amplitude by outer amplitude and subtracting outer phase from inner phase, respectively. Uncertainty in each individual measurement of k is estimated to be around 5 % (Xu et al., 2004). After each experiment, a cross section normal to the axis of the sample cylinder was made in order to determine the distance between the two thermocouples. The thermal diffusivity is then found as the mean of the values determined for each frequency.

In experiments where thermal diffusivity was found to depend on the modulation frequency due to axial end-effects (interference from top and bottom of the cylinder) we determined the limiting diffusivity at infinite frequency D_∞ through fitting the relation

$$D = D_\infty + A_0 \exp(A_1 f), \tag{S5}$$

to our results. In some instances the data is scattered such that the optimal D_∞ value is very different from the data. Where this is the case, we determine the mean diffusivity instead. This is the case for amplitude ratio data in Fig. S5 and phase lag data in Fig. S6. There are also some cases where the data is scattered such that

Eq. S5 does not provide a reliable fit, or where the optimal D_∞ is indistinguisable from the mean. Here again we choose to use the mean diffusivity. This is the case for phase lag data in Figs. S4, S7 and S8.

Where diffusivity values thus derived differ for amplitude ratio and phase lag, the differences cannot be only accounted for by only the additional radiative transfer of heat. These differences likely arise due to scatter in the frequency dependent diffusivity data, so that the mean diffusivity values do not correctly reflect the true values. Based on the differences between phase lag and amplitude ration values, we estimate these discrapancies to be less than 10%, within our final estimates of uncertainty (see text).

S3 Thermodynamic Treatment

We use a Mie-Grüneisen formulation for the Helmholtz free energy F to construct thermodynamic models for each of the phases considered in our measurements (Ita and Stixrude, 1992; Stixrude and Lithgow-Bertelloni, 2005). This approach which ensures that all thermodynamic information can be derived self-consistently by Legendre transformations and differentiation (Callen, 1985). The relation for a single phase is

$$F = F_0(V_0, T_0) + F_c(V, T_0) + F_{th}(V, T) - F_{th}(V, T_0), \tag{S6}$$

where F_c describes isothermal compression

$$F_c(V, T_0) = \frac{9K_0V_0}{2}\left[f^2 + a_1 f^3\right], \tag{S7}$$

$$f = \frac{1}{2}\left[\left(\frac{V_0}{V}\right)^{\frac{2}{3}} - 1\right];\ a_1 = (K_0' - 4), \tag{S8}$$

and F_{th} describes isochoric heating in the quasiharmonic approximation

$$F_{th}(V, T) = 9NR\left(\frac{T}{\theta}\right)^3 \int_0^{\frac{\theta}{T}} x^2 \ln\left[1 - \exp(-x)\right] dx. \tag{S9}$$

The Debye temperature at volume V is obtained as

$$\theta = \theta_0 \exp\left[-\int_{V_0}^{V} \gamma(V')/V' dV'\right], \tag{S10}$$

with $\gamma(V)$ expressed through the finite strain based form of Stixrude and Lithgow-Bertelloni (2005)

$$\gamma = \frac{\gamma_0' + (2\gamma_0' + \gamma_1')\, f + 2\gamma_1' f^2}{3\,(2 + 2\gamma_0' f + \gamma_1' f^2)}, \tag{S11}$$

γ_0' and γ_1' being constants with

$$\gamma_0 = \frac{1}{6}\gamma_0'; \quad q_0 = \frac{\gamma_1' + 2\gamma_0' - \gamma_0'^2}{-3\gamma_0'}. \tag{S12}$$

This expression allows q to vary with density; first principles computations have shown it to better represent $\gamma(V)$ compared to the more commonly used constant-q approximation (de Koker and Stixrude, 2009; Stixrude and Lithgow-Bertelloni, 2005; Oganov and Dorogokupets, 2003; Karki et al., 2000; Anderson, 1974).

Intermediate compositions are represented through free energy mixtures of models for endmembers MgO and FeO for ferropericlase, and $MgSiO_3$, $FeSiO_3$ and $AlAlO_3$ for perovskite. Parameters used in representing each of these phases are taken from the database of Xu et al. (2008).

S4 Experimental Data

Thermal conductivities determined using amplitude ratio as well as phase lag are shown for each of the nine experiments in Figures S3 - S20. To avoid including effects due to direct thermal transfer, we use the amplitude ratio results in our modeling of the temperature dependence (Table 1). Agreement between k values determined from phase lag and from amplitude ratio values are generally within the experimental uncertainty, except for the Fe and Al containing silicate perovskite samples, where k values derived from phase lag are higher than values derived from the amplitude ratio. This likely results from the fact that k in these samples is rather low, so that the contribution from direct radiative transfer seen in the phase lag signal is amplified.

Table S1: Parameters for the Mie-Grüneisen expression of the Helmholtz free energy, at ambient pressure and $T_0 = 300$ K. Taken from Xu et al. (2008)

	V_0 (cm^3/mol)	K_0 (GPa)	K_0'	θ_0 (K)	γ_0	q_0
MgO	11.24	161	3.9	772	1.48	1.6
FeO	12.26	179	4.9	454	1.54	1.6
$MgSiO_3$	24.45	251	4.1	901	1.44	1.4
$FeSiO_3$	25.40	272	4.1	765	1.44	1.4
$AlAlO_3$	25.49	228	4.1	886	1.44	1.4

Table S2: Thermal diffusivity in MgO

P (GPa)	T (K)	D_Φ (mm^2/s)	D_Θ (mm^2/s)
8	373	10.44 ± 0.28	9.57 ± 0.24
8	473	7.76 ± 0.19	7.15 ± 0.18
8	573	6.20 ± 0.16	5.80 ± 0.15
8	673	5.27 ± 0.13	4.86 ± 0.12
8	773	4.49 ± 0.11	4.30 ± 0.11
8	873	3.94 ± 0.10	3.79 ± 0.09
8	973	3.53 ± 0.09	3.38 ± 0.08
8	1073	3.18 ± 0.08	3.03 ± 0.08
8	1173	2.93 ± 0.07	2.75 ± 0.07
8	1273	2.75 ± 0.07	2.48 ± 0.06
14	373	12.58 ± 0.35	11.73 ± 0.30
14	473	9.35 ± 0.32	8.16 ± 0.26
14	573	7.61 ± 0.20	7.20 ± 0.19
14	673	6.38 ± 0.24	6.02 ± 0.15
14	773	5.44 ± 0.16	5.34 ± 0.13
14	873	4.79 ± 0.13	4.76 ± 0.12
14	973	4.32 ± 0.11	4.19 ± 0.10
14	1073	3.88 ± 0.01	3.76 ± 0.09
14	1173	3.57 ± 0.05	3.43 ± 0.09
14	1273	3.34 ± 0.05	3.08 ± 0.08

Table S3: Thermal diffusivity in $Mg_{0.95}Fe_{0.05}O$

P (GPa)	T (K)	D_Φ (mm^2/s)	D_Θ (mm^2/s)
8	373	2.51 ± 0.53	2.95 ± 0.36
8	473	2.00 ± 0.07	2.52 ± 0.34
8	573	1.82 ± 0.06	2.26 ± 0.27
8	673	1.64 ± 0.08	2.05 ± 0.21
8	773	1.62 ± 0.05	1.92 ± 0.18
8	873	1.53 ± 0.06	1.81 ± 0.13
8	973	1.43 ± 0.04	1.70 ± 0.11
8	1073	1.36 ± 0.04	1.54 ± 0.04
14	373	3.81 ± 0.14	3.32 ± 0.09
14	473	3.27 ± 0.20	3.03 ± 0.08
14	573	2.98 ± 0.05	2.82 ± 0.07
14	673	2.72 ± 0.17	2.64 ± 0.07
14	773	2.40 ± 0.08	2.47 ± 0.06
14	873	2.19 ± 0.07	2.28 ± 0.06
14	973	2.03 ± 0.05	2.22 ± 0.06
14	1073	1.87 ± 0.05	2.11 ± 0.05
14	1173	1.76 ± 0.04	1.98 ± 0.05
14	1273	1.59 ± 0.04	1.89 ± 0.05

Table S4: Thermal diffusivity in $Mg_{0.80}Fe_{0.20}O$

P (GPa)	T (K)	D_Φ (mm^2/s)	D_Θ (mm^2/s)
8	373	2.14 ± 0.26	1.98 ± 0.20
8	473	1.78 ± 0.18	1.68 ± 0.21
8	573	1.58 ± 0.15	1.50 ± 0.21
8	673	1.45 ± 0.13	1.39 ± 0.20
8	773	1.38 ± 0.16	1.30 ± 0.18
8	873	1.34 ± 0.12	1.26 ± 0.17
8	973	1.26 ± 0.09	1.18 ± 0.18
8	1073	1.21 ± 0.11	1.12 ± 0.19
8	1173	1.19 ± 0.11	1.05 ± 0.18
14	373	3.08 ± 0.63	1.93 ± 0.05
14	473	2.54 ± 0.41	1.81 ± 0.05
14	573	2.22 ± 0.31	1.69 ± 0.01
14	673	1.98 ± 0.20	1.61 ± 0.05
14	773	1.80 ± 0.21	1.51 ± 0.08
14	873	1.73 ± 0.19	1.50 ± 0.13
14	973	1.61 ± 0.18	1.40 ± 0.12
14	1073	1.54 ± 0.26	1.31 ± 0.10
14	1173	1.48 ± 0.20	1.20 ± 0.12
14	1273	1.42 ± 0.16	1.11 ± 0.12

Table S5: Thermal diffusivity in $MgSiO_3$

P (GPa)	T (K)	D_Φ (mm^2/s)	D_Θ (mm^2/s)
26	473	3.37 ± 0.24	3.47 ± 0.10
26	573	2.90 ± 0.09	2.90 ± 0.08
26	673	2.58 ± 0.12	2.55 ± 0.07
26	773	2.38 ± 0.10	2.30 ± 0.06
26	873	2.23 ± 0.07	2.13 ± 0.06
26	973	2.11 ± 0.07	1.99 ± 0.05
26	1073	2.02 ± 0.08	1.93 ± 0.05

Table S6: Thermal diffusivity in $MgSiO_3$ + 3% $FeSiO_3$

P (GPa)	T (K)	D_Φ (mm^2/s)	D_Θ (mm^2/s)
26	573	1.29 ± 0.28	0.95 ± 0.03
26	673	1.17 ± 0.52	0.90 ± 0.02
26	773	1.03 ± 0.19	0.85 ± 0.02
26	873	1.06 ± 0.19	0.77 ± 0.02
26	973	1.06 ± 0.20	0.77 ± 0.02

Table S7: Thermal diffusivity in $MgSiO_3$ + 2% $AlAlO_3$

P (GPa)	T (K)	D_Φ (mm^2/s)	D_Θ (mm^2/s)
26	573	1.09 ± 0.03	0.79 ± 0.02
26	673	0.93 ± 0.02	0.74 ± 0.02
26	773	0.89 ± 0.02	0.70 ± 0.02
26	873	0.88 ± 0.03	0.66 ± 0.02
26	973	0.92 ± 0.03	0.61 ± 0.02

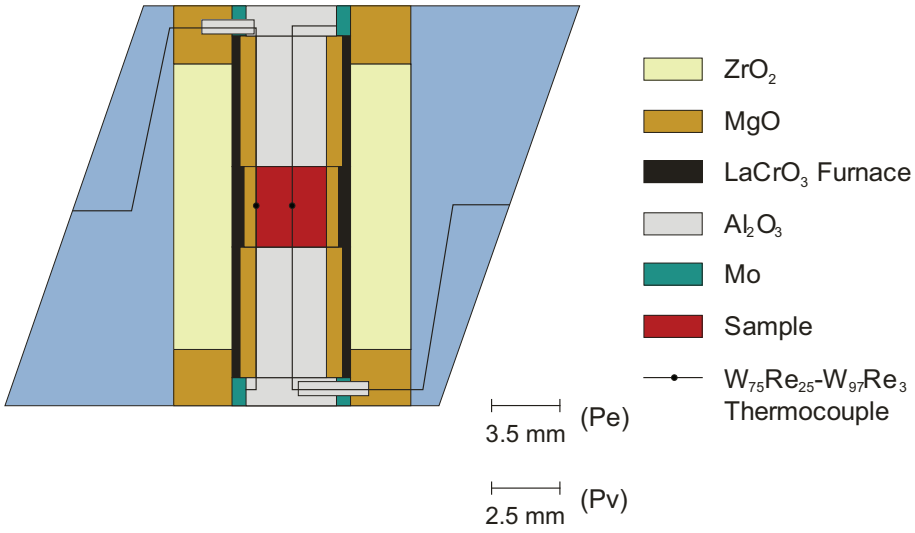

Figure S1: Schematic cross section of the high-pressure cell assembly for the thermal conductivity measurements. The ferropericlase samples used for the measurements at 8 and 14 GPa were 3.5 mm in length and diameter, while a smaller assembly with sample dimensions of 2.5 mm was needed to reach the 26 GPa pressure required for the silicate perovskite measurements.

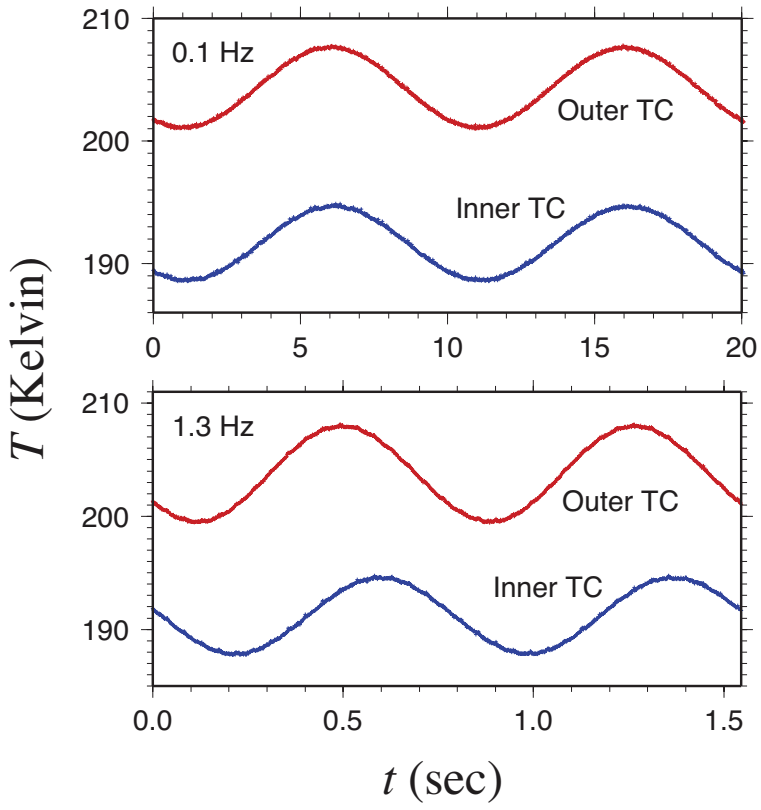

Figure S2: Examples of recorded temperature waves for $MgSiO_3$ perovskite at frequencies of 0.1 and 1.3 Hz. At each temperature 10 cycles were collected, for a total of 2048 data points. Temperature readings of the outer thermocouple is always greater than that of the inner thermocouple; at the highest temperatures this difference reached a maximum of 30 K.

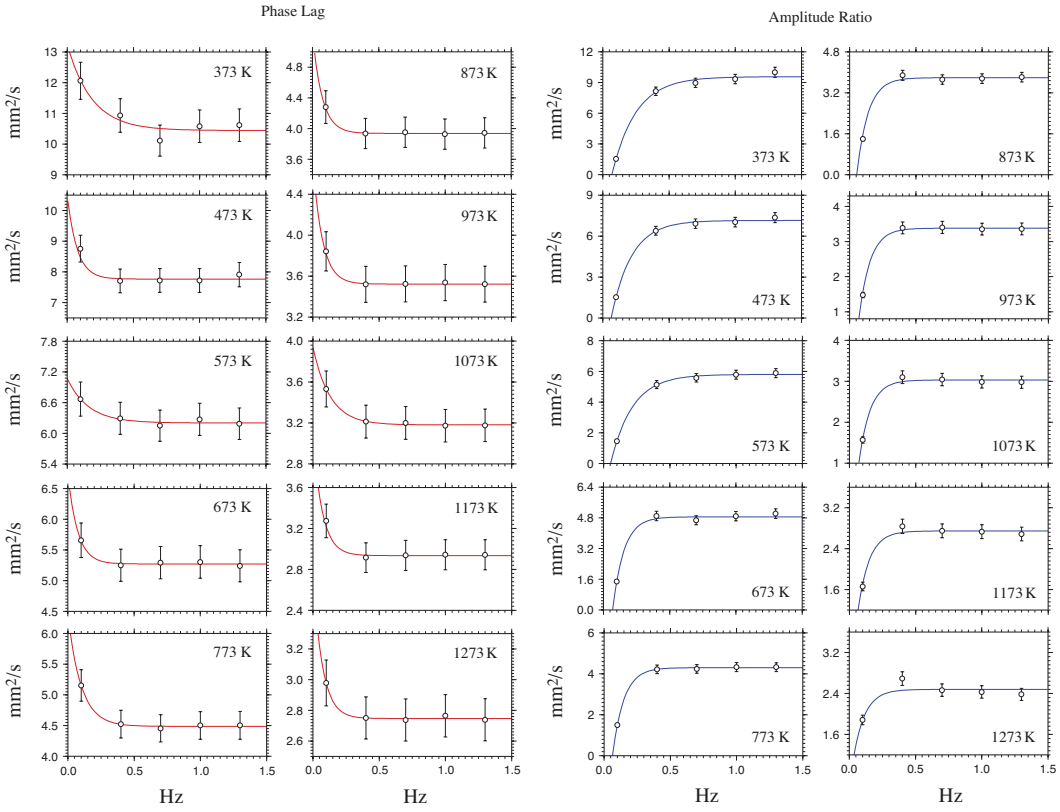

Figure S3: Thermal diffusivity of MgO at 8 GPa as a function of frequency, determined from phase lag and amplitude ratio measurements.

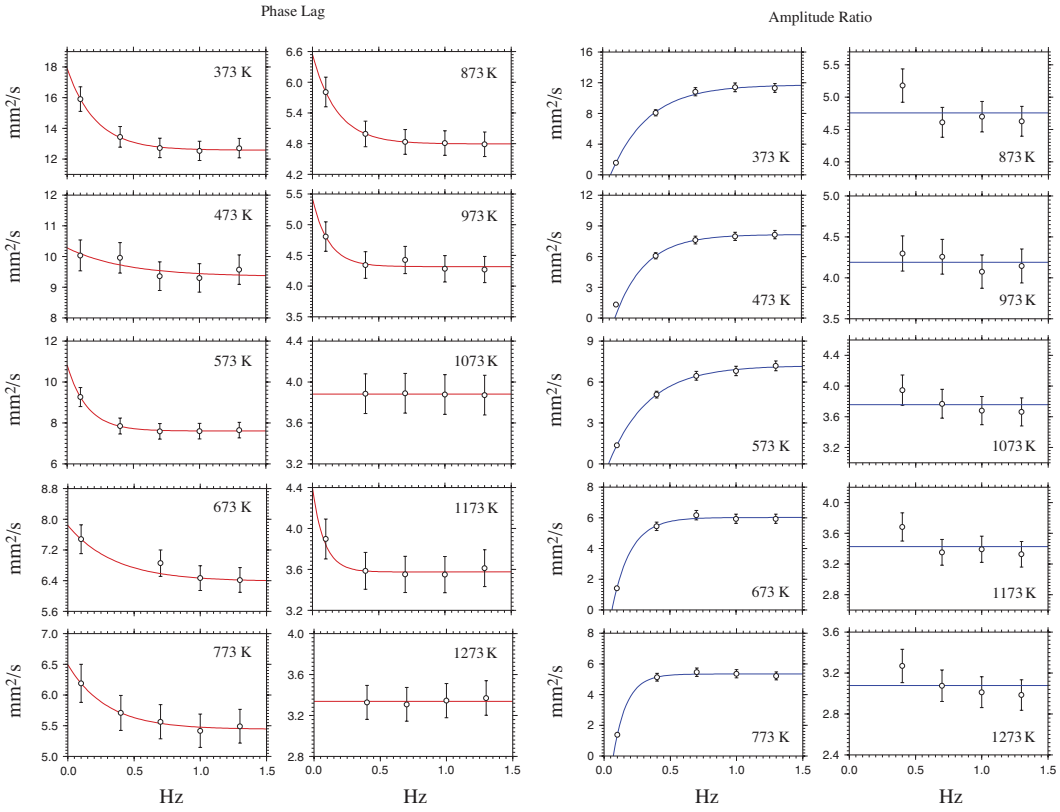

Figure S4: Thermal diffusivity of MgO at 14 GPa as a function of frequency, determined from phase lag and amplitude ratio measurements.

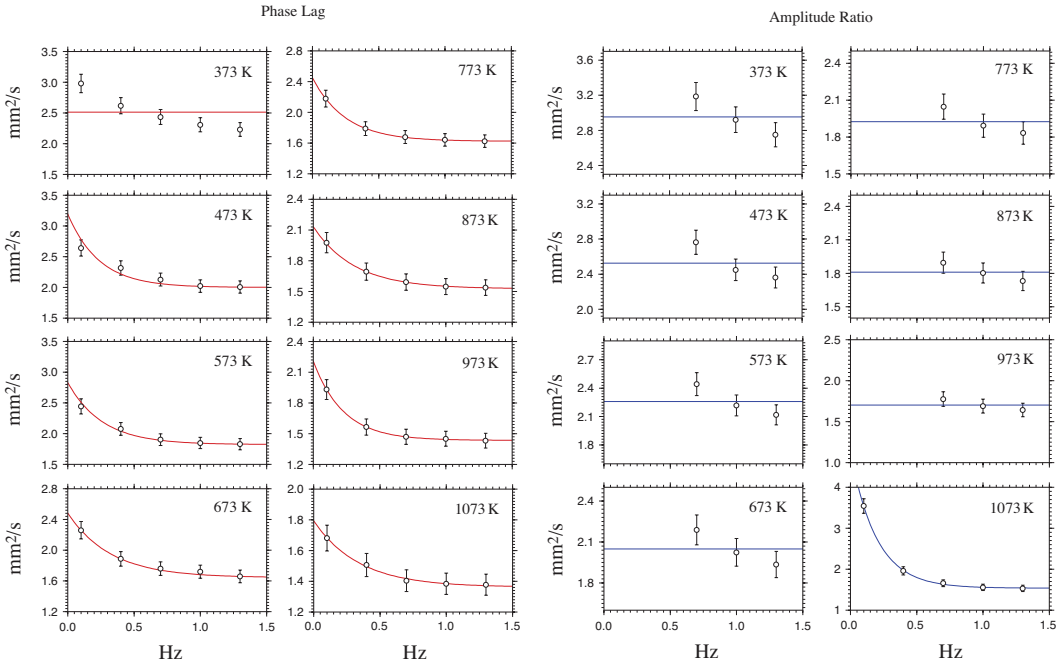

Figure S5: Thermal diffusivity of $Mg_{0.95}Fe_{0.05}O$ at 8 GPa as a function of frequency, determined from phase lag and amplitude ratio measurements.

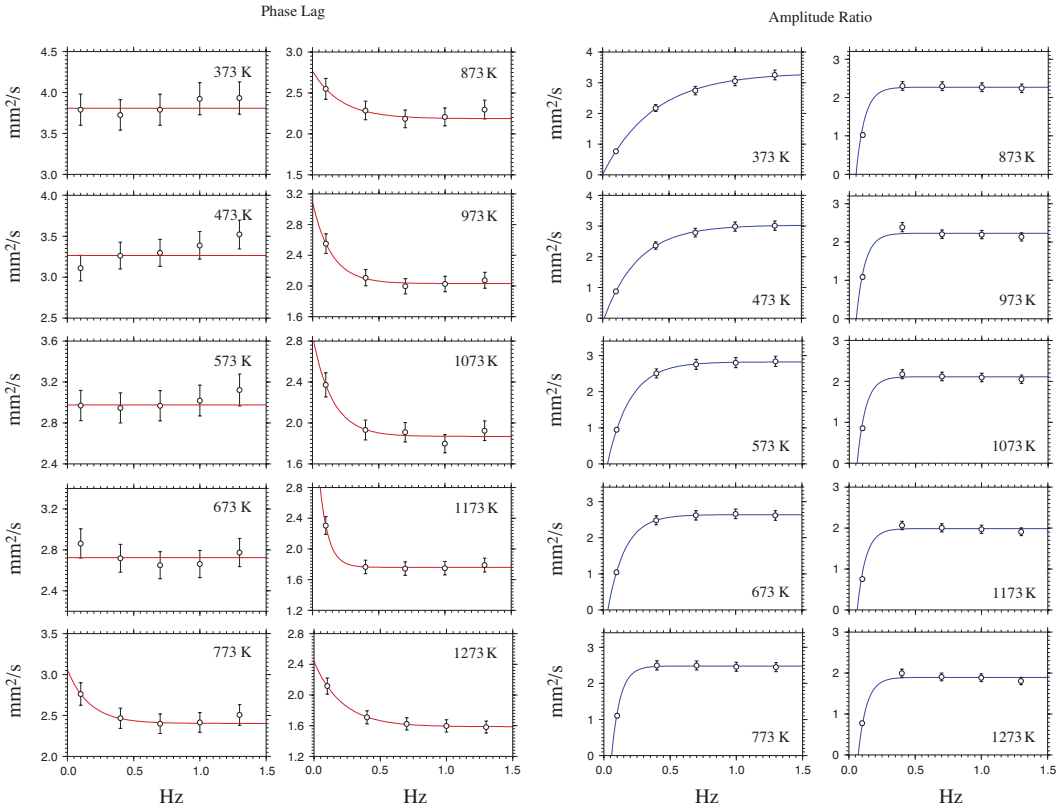

Figure S6: Thermal diffusivity of $Mg_{0.95}Fe_{0.05}O$ at 14 GPa as a function of frequency, determined from phase lag and amplitude ratio measurements.

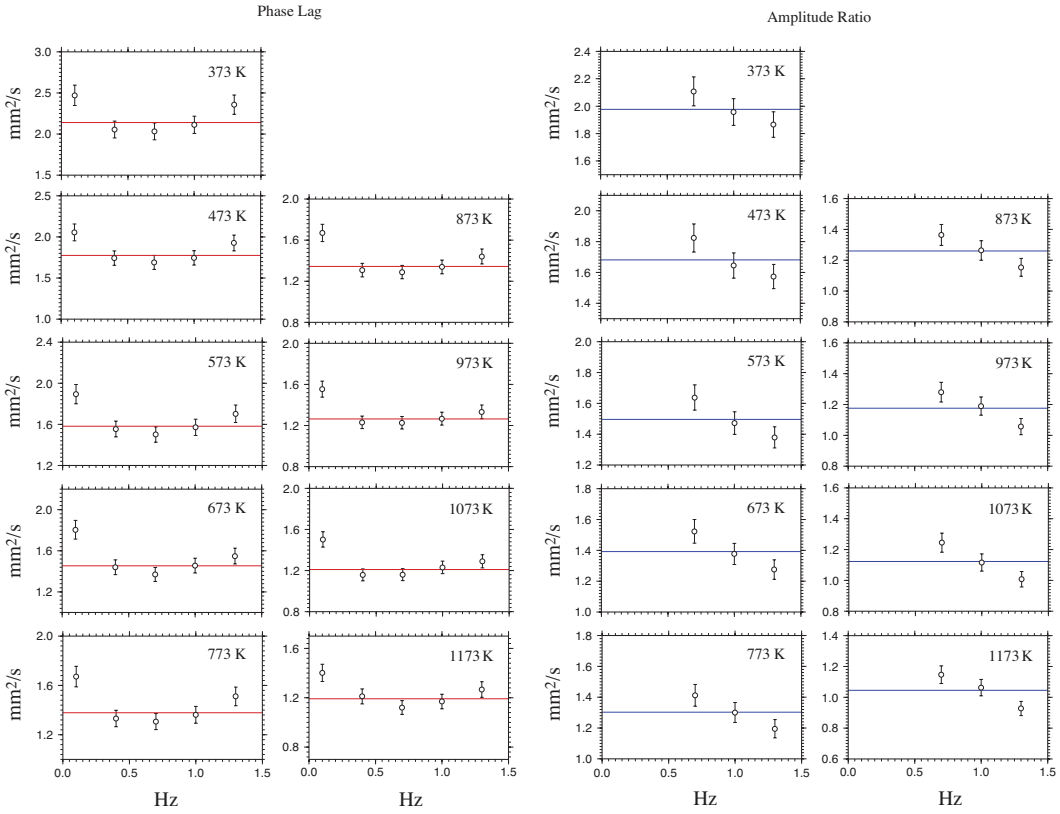

Figure S7: Thermal diffusivity of $Mg_{0.80}Fe_{0.20}O$ at 8 GPa as a function of frequency, determined from phase lag and amplitude ratio measurements.

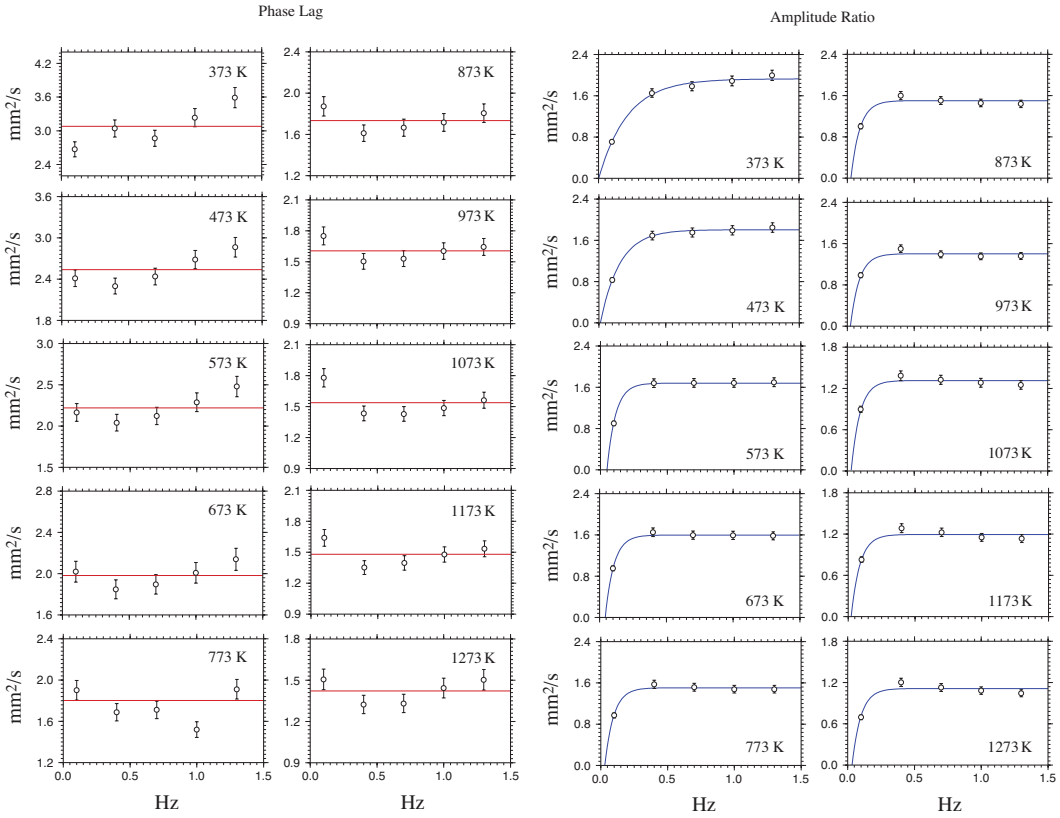

Figure S8: Thermal diffusivity of $Mg_{0.80}Fe_{0.20}O$ at 14 GPa as a function of frequency, determined from phase lag and amplitude ratio measurements.

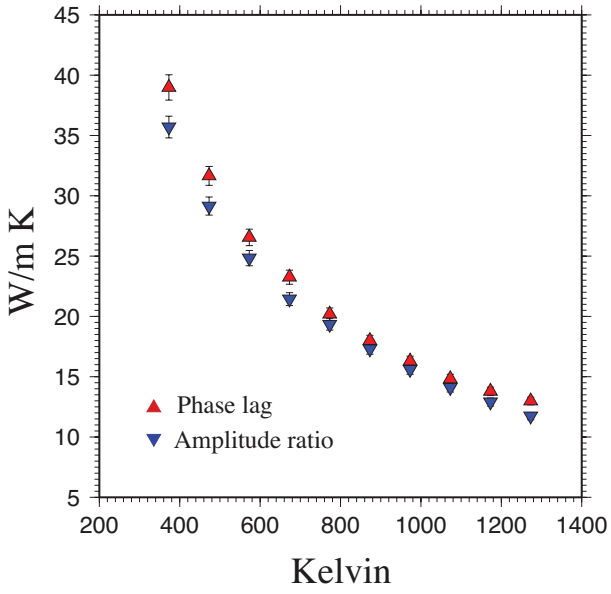

Figure S9: Thermal conductivity of MgO at 8 GPa, determined from phase lag and amplitude ratio diffusivity values.

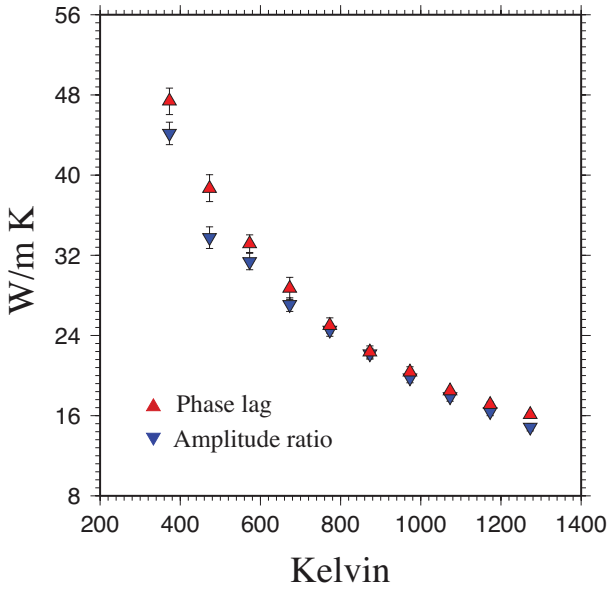

Figure S10: Thermal conductivity of MgO at 14 GPa, determined from phase lag and amplitude ratio diffusivity values.

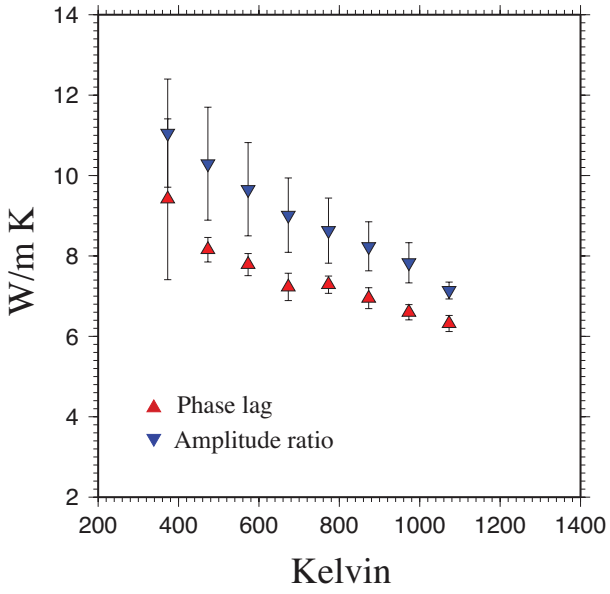

Figure S11: Thermal conductivity of $Mg_{0.95}Fe_{0.05}O$ at 8 GPa, determined from phase lag and amplitude ratio diffusivity values.

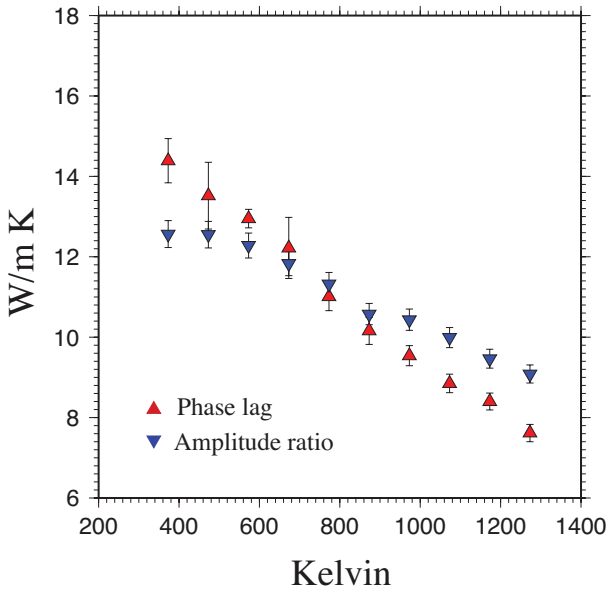

Figure S12: Thermal conductivity of $Mg_{0.95}Fe_{0.05}O$ at 14 GPa, determined from phase lag and amplitude ratio diffusivity values.

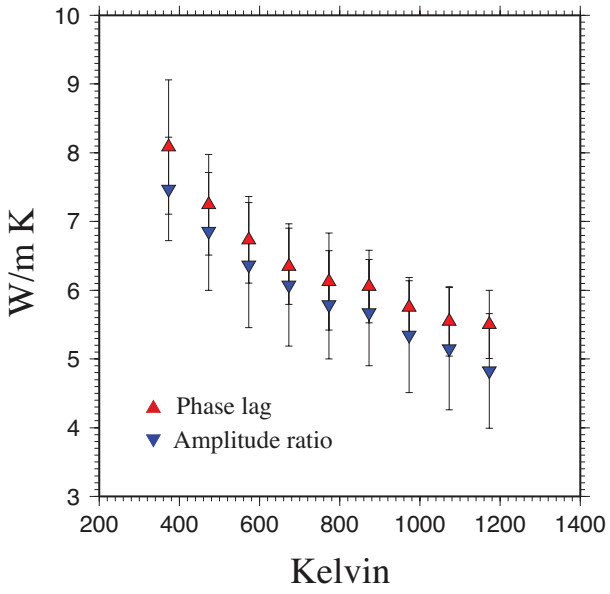

Figure S13: Thermal conductivity of $Mg_{0.80}Fe_{0.20}O$ at 8 GPa, determined from phase lag and amplitude ratio diffusivity values.

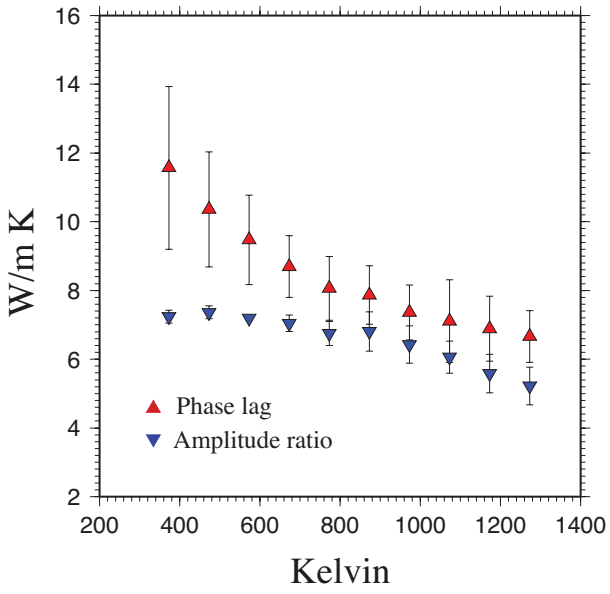

Figure S14: Thermal conductivity of $Mg_{0.80}Fe_{0.20}O$ at 14 GPa, determined from phase lag and amplitude ratio diffusivity values.

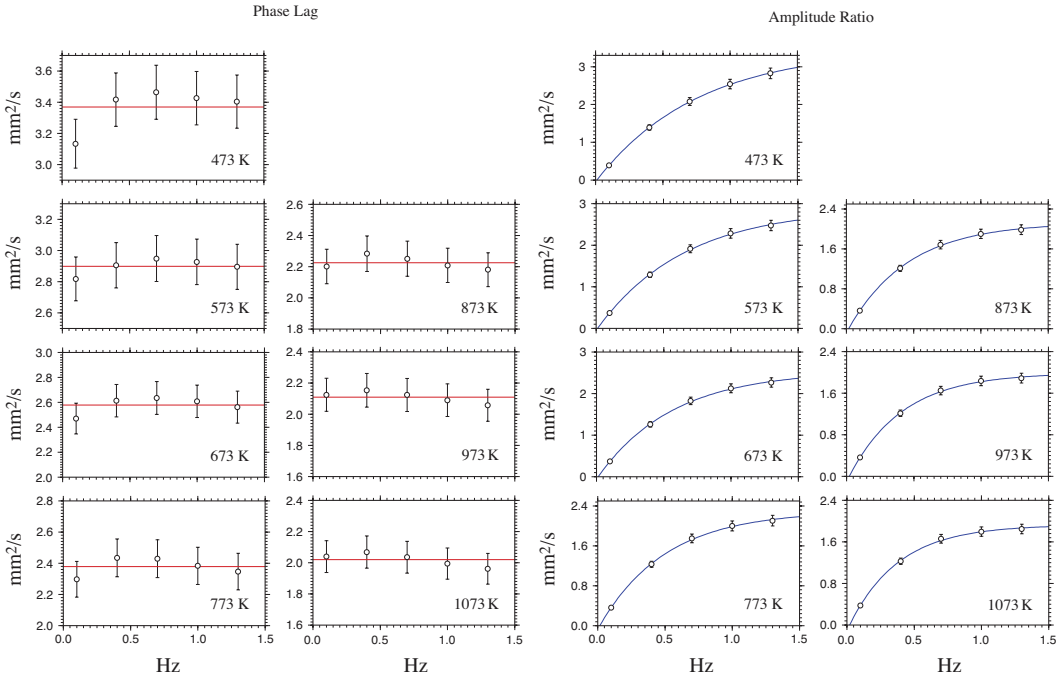

Figure S15: Thermal diffusivity of $MgSiO_3$ perovskite at 26 GPa as a function of frequency, determined from phase lag and amplitude ratio measurements.

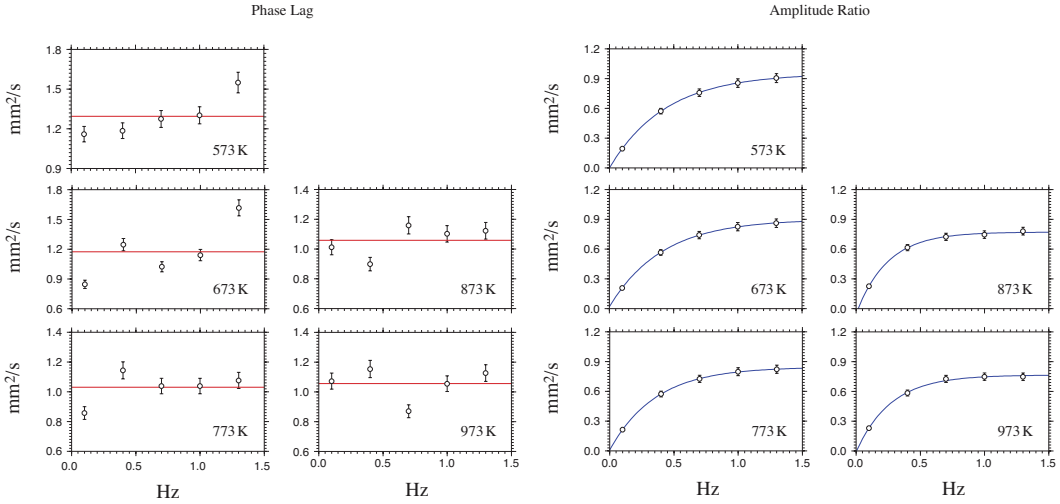

Figure S16: Thermal diffusivity of $MgSiO_3$ + 3% $FeSiO_3$ perovskite at 26 GPa as a function of frequency, determined from phase lag and amplitude ratio measurements.

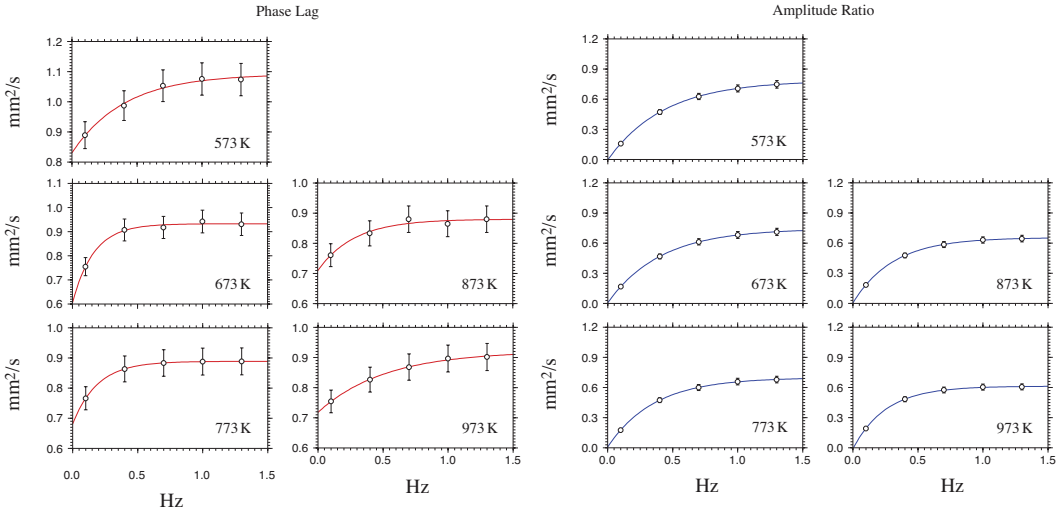

Figure S17: Thermal diffusivity of $MgSiO_3$ + 2% $AlAlO_3$ perovskite at 26 GPa as a function of frequency, determined from phase lag and amplitude ratio measurements.

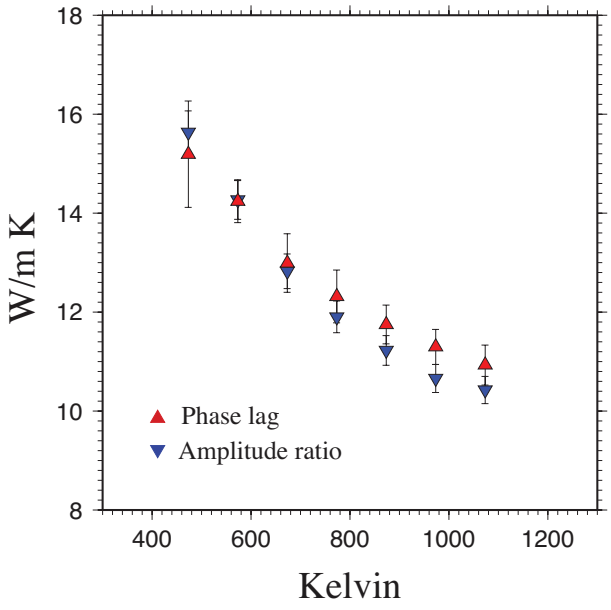

Figure S18: Thermal conductivity of $MgSiO_3$ perovskite at 26 GPa, determined from phase lag and amplitude ratio diffusivity values.

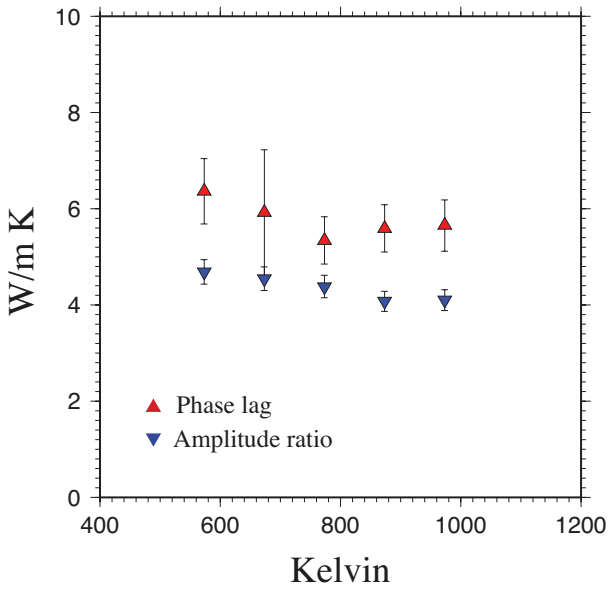

Figure S19: Thermal conductivity of $MgSiO_3$ + 3% $FeSiO_3$ perovskite at 26 GPa, determined from phase lag and amplitude ratio diffusivity values.

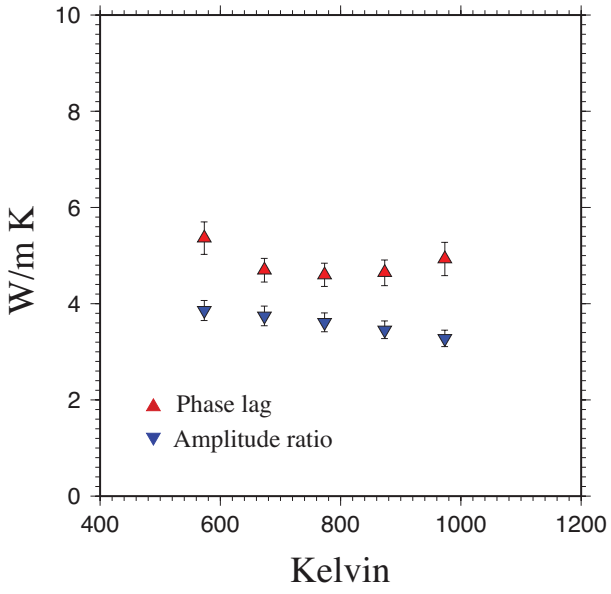

Figure S20: Thermal conductivity of $MgSiO_3$ + 2% $AlAlO_3$ perovskite at 26 GPa, determined from phase lag and amplitude ratio diffusivity values.

References

Anderson O.L. (1974) The Determination of the Volume Dependence of the Grüneisen Parameter γ. *Journal of Geophysical Research* **79**, 1153–1155.

Callen H.B. (1985) *Thermodynamics and an Introduction to Thermostatistics*. John Wiley & Sons, New York, 2nd edition.

de Koker N. and Stixrude L. (2009) Self-Consistent Thermodynamic Description of Silicate Liquids, with Application to Shock Melting of MgO Periclase and $MgSiO_3$ Perovskite. *Geophysical Journal International* **178**, 162–179.

Frost D., Poe B., Trønnes R., Liebske C., Duba A. and Rubie D. (2004) A new large-volume 6-8 multianvil system. *Physics of the Earth and Planetary Interiors* **143-144**, 507–514.

Fujisawa H.a., Fujii N., Mizutani H., Kanamori H. and Akimoto S. (1968) Thermal diffusivity of Mg_2SiO_4, Fe_2SiO_4 and NaCl at high pressures and temperatures. *Journal of Geophysical Research* **73**, 4727–4733.

Ita J. and Stixrude L. (1992) Petrology, Elasticity, and Composition of the Mantle Transition Zone. *Journal of Geophysical Research* **97**, 6849–6866.

Karki B.B., Wentzcovitch R.M., De Gironcoli S. and Baroni S. (2000) High-pressure lattice dynamics and thermoelasticity of MgO. *Physical Review B* **61**, 8793–8800.

Oganov A.R. and Dorogokupets P.I. (2003) All-electron and pseudopotential study of MgO: Equation of state, anharmonicity, and stability. *Physical Review B* **67**, doi: 10.1103/PhysRevB.67.224110.

Stixrude L. and Lithgow-Bertelloni C. (2005) Thermodynamics of mantle minerals - I. Physical properties. *Geophysical Journal International* **162**, 610–632.

Xu W., Lithgow-Bertelloni C. and Stixrude L. (2008) The effect of bulk composition and temperature on mantle seismic structure. *Earth and Planetary Science Letters* **275**, 70–79.

Xu Y., Shankland T.J., Linhardt S., Rubie D.C., Langenhorst F. and Klasinksi K. (2004) Thermal diffusivity and conductivity of olivine, wadsleyite and ringwoodite to 20 GPa and 1373 K. *Physics of the Earth and Planetary Interiors* **143-144**, 321–326.

159 Zhang S. and Jin J. (1996) *Computation of Special Functions*. John Wiley & Sons,
160 New York.